Citation for final published version:

Bose, Manjith, Creedon, Daniel L., Barlow, Anders, Stuiber, Michael, Klemencic, Georgina M. , Mandal, Soumen , Williams, Oliver , van Riessen, Grant and Pakes, Christopher I. 2022. Low-noise diamond-based D.C. nano-SQUIDs. ACS Applied Electronic Materials 4 (5) , pp. 2246-2252. 10.1021/acsaelm.2c00048

Publishers page: http://dx.doi.org/10.1021/acsaelm.2c00048

Low-noise diamond-based D.C. nano-SQUIDs

M. Bose,[1,a)] D. L. Creedon,[2] A. Barlow,[3] M. Stuiber,[4] G. Klemenic,[5] S. Mandal,[5] O. A. Williams,[5] G. van Riessen,[1] and C. I. Pakes[1,b)]

[1]*Department of Chemistry and Physics, La Trobe University, Bundoora, Victoria 3086, Australia*

[2]*School of Physics, The University of Melbourne, Victoria 3010, Australia*

[3] *Materials Characterisation and Fabrication Platform, The University of Melbourne, Victoria 3010, Australia*

[4]*Melbourne Centre for Nanofabrication, 151 Wellington Road, Clayton, Victoria 3168, Australia*

[5]*School of Physics and Astronomy, Cardiff University, Cardiff CF24 3AA, United Kingdom*

Nanoscale superconducting quantum interference devices (nano-SQUIDs) with Dayem bridge junctions and a physical loop size of 50 nm have been engineered in boron-doped nanocrystalline diamond films using precision Ne-ion beam milling. In an un-shunted device, non-hysteretic operation can be maintained in an applied field exceeding 0.1 T with a high flux-to-voltage transfer function, giving a low flux noise $\phi_{noise} = 0.93\,\mu\phi_0/\sqrt{\mathrm{Hz}}$ at 10 kHz, and concurrent spin sensitivity of 7 $\mathrm{spins}/\sqrt{\mathrm{Hz}}$. At elevated magnetic fields, up to 2 T, flux modulation of the nanoSQUID output voltage is maintained but with an increase in period, attributed to an additional phase bias induced on the nanoSQUID loop by up to 16 vortices per period penetrating the nanoSQUID electrodes.

Nanoscale superconducting quantum interference devices (nano-SQUIDs) are considered a promising tool for achieving the goal of single electron spin detection on account of their performance as a flux-to-voltage transformer and low sensitivity to external flux noise.[1] Over the last two decades a wide range of nano-SQUIDs have been demonstrated using a variety of materials,[2–4] device geometries and fabrication techniques.[5–8] Many of these have exploited weak-links formed using Dayem bridges, which are desirable due to their low capacitance, high current density and insensitivity to in-plane magnetic fields, suitable for high magnetic field applications. [9,10] However, reported operational magnetic fields so far for nano-SQUIDs are below 1 T.[10] Superconducting diamond, achieved through boron doping with a density exceeding 4.5 x 10^{20} cm^{-3},[11] is considered an excellent candidate for D.C. SQUID technology because of its high critical field and critical current density. A micrometre sized D.C. SQUID has been demonstrated using thin-film, boron-doped nanocrystalline diamond (NCD) with a Dayem bridge architecture and loop size of 2.5 μm,[12] reporting operation in an applied magnetic field up to 4 T, and a flux noise sensitivity of $4 \times 10^{-5}\ \Phi_0/\sqrt{\mathrm{Hz}}$ in an applied field of 0.3 mT. Recently, a D.C. SQUID was also demonstrated using boron-doped single crystal diamond (SCD), taking a new approach to fabricating Josephson junctions at a regrowth-induced step-edge, and with a loop size of 32 μm.[13] It is well known that the spin sensitivity of D.C. SQUIDs can be improved by reducing their loop area, which reduces the inductance of the SQUID loop and hence sensitivity to external flux noise is reduced.[14] Here, we present diamond-based D.C. nano-SQUIDs with a loop area well below 1 μm^2, operating at a temperature up to 2 K and in an applied magnetic field up to 2 T. The devices were fabricated using boron-doped NCD thin- films, with the SQUID loop and Dayem bridge weak-links engineered using a precision Ne ion-probe, capable of milling to better than 30 nm precision. The electronic properties and spectral noise density of devices with and without a metallic (Au) shunt layer are examined in detail. Extremely low noise properties can be achieved, with a flux noise of 0.93 $\mu\phi_0/\sqrt{\mathrm{Hz}}$ and spin sensitivity of 7 $\mathrm{spins}/\sqrt{\mathrm{Hz}}$ demonstrated for these devices.

Devices were fabricated using a boron-doped NCD film, of thickness 330 nm, grown using microwave plasma enhanced chemical vapor deposition (MPCVD) technique (SEKI-ASTeX 6500 series reactor) on a silicon substrate with a 500 nm thick SiO_2 buffer layer. The superconducting transition temperature of the film, was found to be ~ 3 K, suggesting a boron concentration of approximately 2.3 x 10^{21} cm^{-3}.[15] The fabrication of devices involved a two-step process. Firstly, on the NCD film, bridges of width in the range 0.75 – 1 μm and length about 1 μm were defined using electron beam lithography (EBL) and then a Cr (5 nm)/Au (50 nm) layer was deposited on these patterns via e-beam evaporation. After lift-off, the metal layer serves as a mask for the subsequent oxygen plasma etching in a 25-minute RIE process to remove unmasked regions of the diamond surface, in addition to acting as a bond pad. The sample was then mounted in a chip carrier and fabricated bridges wire bonded. Secondly, nano-SQUID devices were engineered on the NCD bridges via Ne-ion probe milling using a ZEISS ORION NanoFab helium ion microscope (HIM). Precision milling of Dayem bridge weak links and SQUID loops were performed using a Ne-ion beam with an energy of 25 keV and a beam current of 0.8 pA, with milling patterns generated using a Fibics NanoPatterning and Visualization Engine (NPVE).

Low temperature transport and noise measurements of nano-SQUIDs have been performed using a Leiden cryogen-free dilution refrigerator operating at temperatures in the range 50 mK to 300 K, and in magnetic fields up to 7 T. Current-voltage (I-V) characteristics were measured in a four-terminal DC configuration using a source-meter unit (Keithley 2450) to determine the critical current (I_c) of the nano-SQUIDs. I-V characteristics of each device were measured as a function of temperature, T, and applied magnetic field, (B_z), in direction normal to the nano-SQUID loop. Spectral noise measurements of the fabricated nano-SQUIDs were obtained using a Liquid Instruments Moku:Lab FPGA-based spectrum analyser.

Prior to fabrication of the nano-SQUIDs, experiments were performed on several devices to examine how the critical current, I_c, of engineered Dayem bridges scales with the bridge dimensions. It was observed that Dayem bridges of length 27 nm were achievable by milling with the Ne-ion beam, limited by the size of the ion beam and ion straggle within the material. Bridges with a physical width of approximately 200 nm were found to operate as a Josephson junction, with $I_c \sim 5\ \mu$A at 50 mK, while bridges with a width smaller that 200 nm exhibited Ohmic current-voltage (*I*-*V*) characteristics, as illustrated in Figure 1 (a). The reproducibility of these findings across several devices suggests that the physical size of the bridge, rather than the underlying granularity of the film, governs the weak-link behaviour. We note that the physical width (200 nm) of the fabricated bridges is significantly larger than the superconducting coherence length ($\xi \sim$ 10 nm), which would be the scale for which a Dayem bridge would be expected to operate as a Josephson junction and will return to consider this later.

The Cr/Au layer plays a critical role in the fabrication and operation of the devices, in addition to serving as a mask for RIE processing as noted above. The metal layer serves as a contact pad for wire bonding the devices, a protective layer for the weak links during Ne-ion milling, and as a resistive shunt for fabricated Dayem bridges and nano-SQUIDs. It was observed that for some devices the metal layer in the vicinity of the weak links was removed during the fabrication process or subsequent handling of devices, presumably due to electrostatic discharge or excessive current density, so that the resistive shunt was removed. Here we report the transport measurements of two nano-SQUID devices with similarly matched physical loop sizes of approximately 50 nm and square geometry, one with the resistive shunt intact (Device A) and one with the shunt layer removed (Device B). Device A was fabricated on a bridge with length and width of 1 μm, Device B was fabricated on a bridge with length 1 μm and width of 0.75 μm; these widths represent the size of the nano-SQUID washer. Figure 1(b) illustrates a secondary electron (SE) image of device A imaged in the HIM.

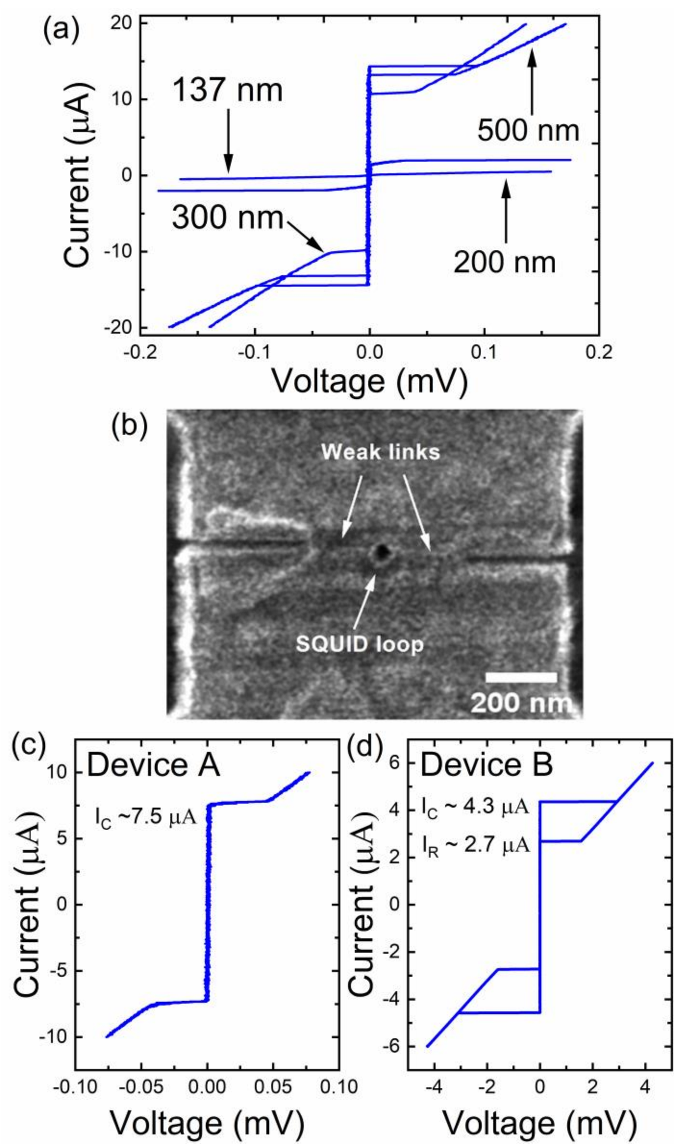

Figure 1. (a) *I*-*V* characteristic of bridges with different weak link widths (b) SEM image of a nano-SQUID device A with square loop of size 50 nm. *I*-*V* characteristics of (c) Device A and (d) Device B, measured at 50 mK, and $B_z = 0$ T, illustrating non-hysteretic and hysteretic behaviour respectively.

I-*V* characteristics for both nano-SQUIDs devices are shown in Figure 1 (c and d). Device A, with a critical current, I_C, of 7.5 μA at 50 mK, was found to exhibit non-hysteretic behaviour at all temperatures and magnetic fields, indicating that the SQUID is overdamped. Device B exhibited hysteretic behavior at 50 mK with I_C = 4.3 μA and a retrapping current, I_R, of 2.7 μA, indicating that the device is underdamped; this is expected for a nanoSQUID without resistive shunts. For Device B, non-hysteretic *I*-*V* characteristics were observed in an applied field, B_z, exceeding 0.1 T, suggesting this device could be used as a stable flux-to-voltage transformer due to its overdamped behaviour at elevated fields.

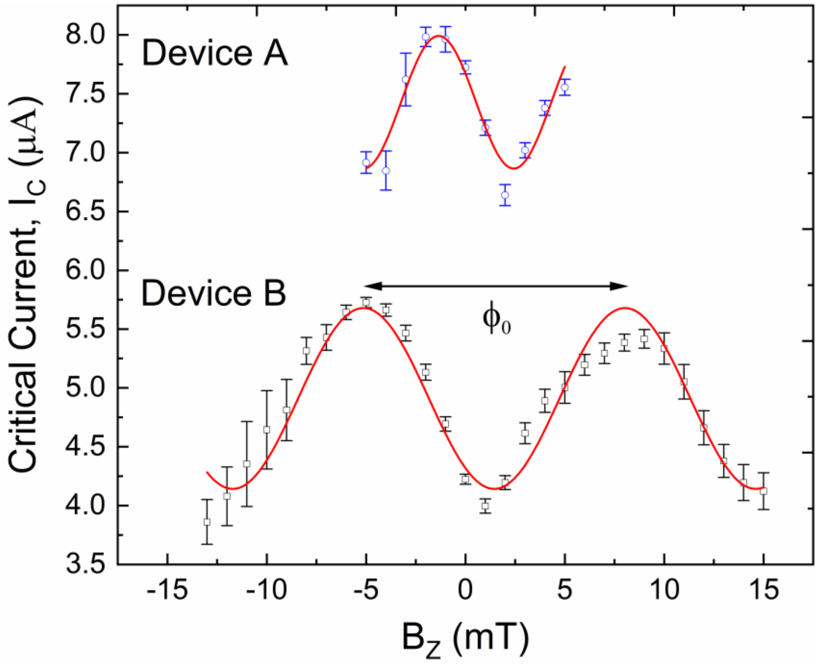

Figure 2. Low field oscillation of I_C as a function of B_z for both nano-SQUIDs at a temperature of 50 mK. The critical current at each magnetic field was averaged over fifty separate *I-V* measurements. The solid lines show sinusoidal fits to the experimental data.

Operation of the devices as D.C. SQUIDs was confirmed by examining the modulation of I_C as a function of B_z, as shown in Figure 2 for $B_z \sim 0$ T. For each applied field, the critical current was obtained from an average of fifty independently measured *I-V* curves. Both devices exhibited sinusoidal oscillation of I_C with B_z, with a period, ΔB_0, of 8 ± 1 mT for Device A and 13 ± 1 mT for Device B, derived from fits to the $I_C - B_z$ data in Fig. 2. For a SQUID of loop size 50 nm the period of oscillation corresponding to a single flux quantum, ϕ_0, is estimated to be about 827 mT, where we simply define $loop\ area = (loop\ size)^2$. The measured periodicity of both devices is considerably smaller than this, suggesting that the effective loop size of the devices is larger than the physical loop size, and differs between the two devices. From the values of B_0 noted above, the effective loop size of the devices was determined to be 508 ± 16 nm for Device A and 399 ± 16 nm for Device B.

The observation of a difference between the physical and effective sizes of the SQUID loop area, and of the width of the Dayem bridges noted earlier, is not unusual for devices engineered using focused ion beams, and has been reported for Nb devices.[16] In the case of Nb, the difference between the physical and effective electronic widths of a Dayem bridge can be understood from the lateral straggle of implanted ions causing modification of the crystal, and a concurrent suppression of superconductivity, in the periphery of milled regions of the material. The effect of ion implantation on superconductivity of boron doped diamond has also been reported.[17] A lateral straggle of only ~ 8 nm is expected for 25 keV Ne ions implanted into diamond,[17] which cannot account for the significant difference between the physical width (200 nm) of the fabricated bridges and the anticipated ~10 nm superconducting diamond core forming the Josephson junction in the present case. We note however that in contrast to metallic Nb Dayem bridges, ion-beam damage in the periphery of diamond bridges may lead to band structure modification in the diamond extending laterally over length scales much larger than the size of the directly damaged region.[18] Positively charged defects created by ion impacts, which lie 1.9 eV above the valence band minimum,[19,20] are known to give rise to hole depletion and band bending of the order of 1 eV, extending several tens of nanometres beyond each ion impact site.[19] This would similarly contribute to the effective SQUID loop size being considerably larger than its physical size.

The flux-to-voltage transfer function, $\partial \mathrm{V}/\partial \phi_{\mathrm{o}}$, can be estimated using the relationship $R_N\, \partial I_C/\partial \phi_{\mathrm{o}}$, where $\partial I_C/\partial \phi_{\mathrm{o}}$ is evaluated from the maximum slope of the fit to the $I_c - B_z$ data (Figure 2), giving 0.15 mA/ϕ_0 for Device A and 0.11 mA/ϕ_0 for Device B. R_N is the normal state resistance, determined from

I-V curves, to be about 12 Ω for Device A and 819 Ω for Device B. The corresponding values of $\partial \mathrm{V}/\partial \phi_{\mathrm{o}}$, are 1.8 $\mathrm{mV}/\phi_{\mathrm{o}}$ for Device A and 95.5 $\mathrm{mV}/\phi_{\mathrm{o}}$ for Device B, the latter being two orders of magnitude higher on account of the higher normal state resistance.

The flux noise was evaluated using $\phi_{noise} = V_{\mathrm{noise}}/(\partial \mathrm{V}/\partial \phi_{\mathrm{o}})$, where the spectral voltage noise, V_{noise}, was measured for each device in the range 1 Hz – 100 kHz using a Liquid Instruments Moku:Lab FPGA-based spectrum analyser. The noise floor of the spectrum analyser was measured to be approximately 70 nV/$\sqrt{\mathrm{Hz}}$, which is considerably higher than the expected voltage noise floor of the nano-SQUIDs, so the output voltage of the devices was amplified by ×100 prior to measurement with the analyser. Figure 3 shows the measured V_{noise} as a function of frequency; both devices have similar noise characteristics with a white noise floor of 4 nV/$\sqrt{\mathrm{Hz}}$ at frequencies exceeding 10 kHz and a voltage noise dominated by $1/f$ noise at lower frequencies. For Device A, $\phi_{noise} = 2.17\ \mu\phi_0/\sqrt{\mathrm{Hz}}$ in the white noise regime at 10 kHz and increases to 3.25 $\mu\phi_0/\sqrt{\mathrm{Hz}}$ at 1 kHz. The corresponding results for Device B were found to be 0.042 $\mu\phi_0/\sqrt{\mathrm{Hz}}$ at 10 kHz and 0.063 $\mu\phi_0/\sqrt{\mathrm{Hz}}$ at 1 kHz. To compare the noise performance of these devices with nano-SQUIDs fabricated using other materials and fabrication techniques, we also estimate the spin sensitivity, expressed in terms of the Bohr magneton, giving a sensitivity $S_n\sim 223\ \mathrm{spins}/\sqrt{\mathrm{Hz}}$ for Device A and $S_n\sim 3\ \mathrm{spins}/\sqrt{\mathrm{Hz}}$ for Device B. While the voltage noise of both devices is similarly matched, the high flux-to-voltage transfer function for Device B, which can be operated in a stable, non-hysteretic regime in applied fields exceeding 0.1 T, gives this device superior noise performance.

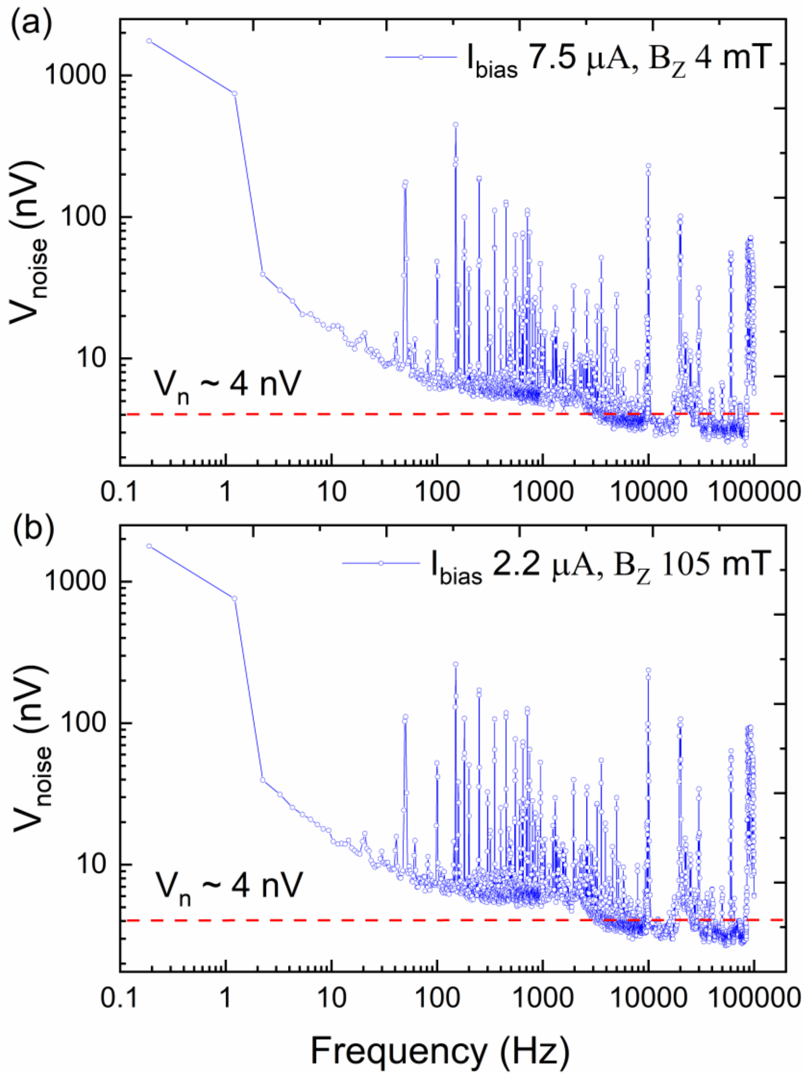

Figure 3. Voltage noise of (a) device A and (b) device B, measured as a function of frequency. Both devices are operated in the non-hysteretic regime during noise measurements. The current bias, operating temperature and magnetic field are indicated in the figure for each case. The peaks in the voltage noise spectrum were attributed to noise from the power supply of the superconducting high-field magnet.

We now turn to a direct measurement of $\partial V/\partial \phi_o$ for Device B and explore its behaviour in higher magnetic fields. To this aim, Device B was operated in a dynamic mode, in which modulation of the output voltage was measured directly as a function of B_z with a fixed bias current optimised to maximise the modulation in the output voltage. The corresponding output curves, obtained at 50 mK, are shown in Figure 4 for applied magnetic fields of approximately 0.1 T, 0.5 T and 1.56 T. For the case of $B_z \sim 0.1$

T, with an applied current bias of 2.2 μA, a transfer function $\partial \mathrm{V}/\partial \phi_{\mathrm{o}}$ = 43 mV/ϕ_{o} was determined; this is a factor of about 2 smaller than the value deduced from $R_N\, \partial I_C/\partial \phi_{\mathrm{o}}$ at $B_z \sim 0$ T. From this direct, more accurate measurement of $\partial \mathrm{V}/\partial \phi_{\mathrm{o}}$, the flux noise is evaluated to be $\phi_{noise} = 0.93\ \mu\phi_0/\sqrt{\mathrm{Hz}}$ at 10 kHz, which corresponds to a spin sensitivity of 7 spins/$\sqrt{\mathrm{Hz}}$. We take this value as the achievable spin sensitivity of Device B and note that it is comparable to the best spin sensitivities reported for other materials: 7 spins/$\sqrt{\mathrm{Hz}}$ reported for Nb/AlOx/Nb cross-type JJ nano-SQUIDs,[4] 4.9 spins/$\sqrt{\mathrm{Hz}}$ reported for a nanoscale three-junction Pb based SQUID-on-tip,[3] and 1.4 spins/$\sqrt{\mathrm{Hz}}$ reported for a Pb nanoSQUID.[2]

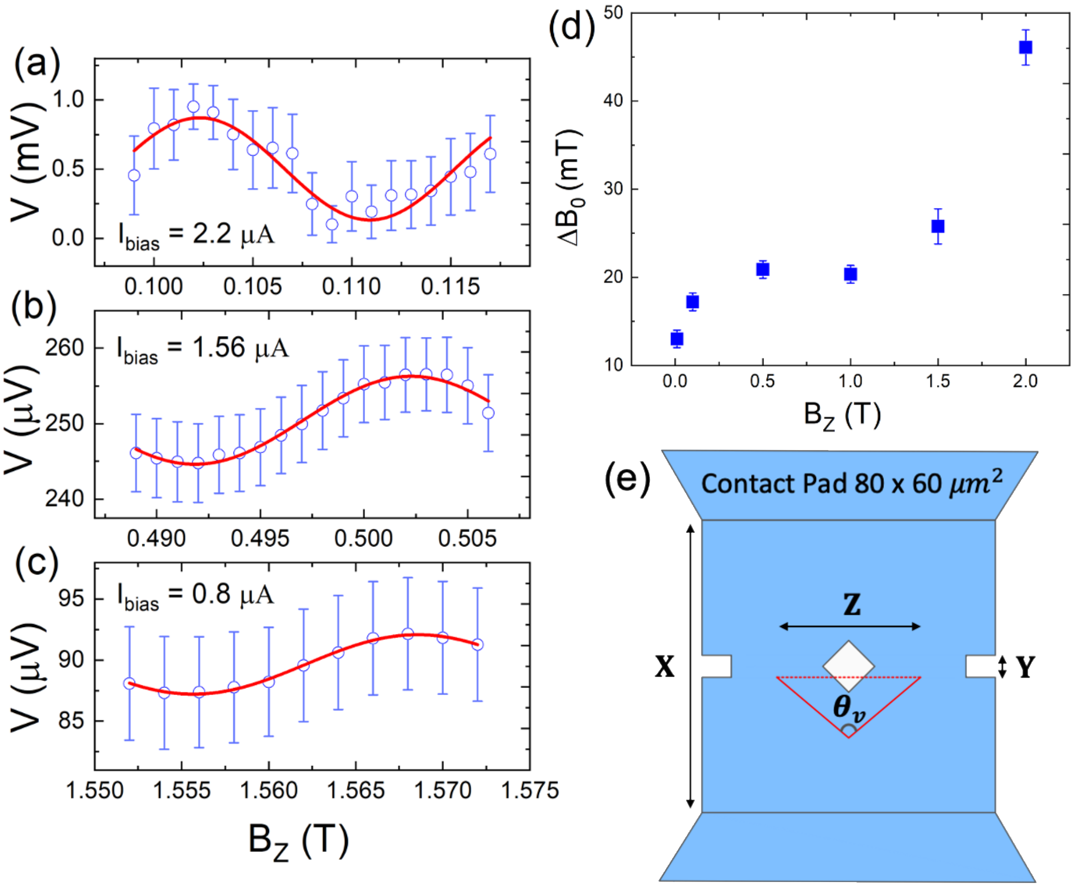

Figure 4 Modulation of the output voltage as a function of magnetic field (B_z) for Device B at 50 mK. B_z is in the range of (a) 0.1 T (b) 0.5 T and (c) 1.5 T. In each case the current bias was optimised to maximise the modulation of output voltage. The period, ΔB_0, of the sinusoidal modulation in the output voltage in each case is shown in (d). The geometrical figure for calculating vortex penetration is shown in (e), where X = 1 μm, Y = 27 nm, and Z = 270 nm.

Figure 4 illustrates an observed decrease in the peak-to-peak modulation of the output voltage as B_Z is increased, as expected, however modulation of the output voltage can still be observed in fields exceeding 1 T. We note that the modulation in the output voltage was too small to measure at temperatures above 2 K and B_Z exceeding 2 T (at an operating temperature of 50 mK). Values of ΔB_0 and the peak-to-peak modulation in output voltage, derived from sinusoidal fits to the experimental data, are summarized in Table I for a variety of measurements at elevated magnetic field and temperature. The period ΔB_0 of the modulation in output voltage is also seen to vary with B_Z, as illustrated in Figure 4(d) in Table I, with a close to three-fold increase in ΔB_0 between B_Z = 0.1 T and B_Z = 2 T. Furthermore, ΔB_0 is observed to decrease, albeit to a much lesser extent, as the temperature is increased for a given field. The observed decrease in ΔB_0 as the temperature is increased at fixed B_Z suggests an increase in the effective area of the nanoSQUID loop as $T \rightarrow T_c$, presumably as superconducting material in the periphery of the nanoSQUID loop becomes normal. For B_Z = 10 mT, we estimate an increase in the effective loop size from 399 ± 16 nm at 50 mK to 455 ± 16 nm nm at 2K.

	10 mT	**0.1 T**	**0.5 T**	**1 T**	**1.5 T**	**2 T**
50 mK	13 ± 1 mT	17 ± 1 mT 800 μV	21 ± 1 mT 10 μV	20 ± 1 mT 6 μV	26 ± 2 mT 5 μV	46 ± 2 mT 3 μV
1 K	13 ± 1 mT	8 ± 1 mT 8.3 μV	15 ± 1 mT 5.05 μV	-	-	-
2 K	10 ± 1 mT 600 μV	-	-	-	-	-

Table. I Observed variation in peak-to-peak modulation of the output voltage (in μV), along with the period, ΔB_0 (in mT), as a function of B_Z for Device B. Note that the device was hysteretic at temperatures of 50 mK and 1 K in an applied field of 10 mT, for which the corresponding values of B_0 were derived from $I_C - B_Z$.

The significant increase in period ΔB_0 as B_Z is increased at fixed temperature can be attributed to an additional phase bias induced on the nanoSQUID loop by Abrikosov vortices entering the superconducting electrodes as the field is increased above the critical field, B_{c1}. We write $\Delta B_0 = B_0 + B_v$, where B_0 is the fixed period in the vortex-free regime ($B_z < B_{c1}$), and B_v represents the change in the period arising from the additional phase change induced by penetration of vortices into the superconducting diamond electrodes at higher applied fields. The measured increase in the period of the modulation in the output voltage can be used to estimate the number of vortices entering the nanoSQUID electrodes for each period of oscillation. Following the approach of Ku *et.al.*,[22] who described the effect of vortex penetration on the flux modulation in Al devices, the average number of vortices entering the electrodes per period at high field can be written as $N = (2\pi/\Delta\varphi_v)\ (B_v/B_0)$, where $\Delta\varphi_v$ is the average phase difference imposed by a single vortex on the nanoSQUID loop. We assume B_0 = 13 mT, the measured period at $B_z \sim 0$ T, while $B_v = \Delta B_0 - B_0$ is the difference between the measured period and B_0 at a given field, as illustrated in Figure 4(d). The phase difference, $\Delta\varphi_v$, is estimated as the phase bias imposed across the nanoSQUID loop by a single vortex located in the centre of one of the diamond electrodes, and is equal to the angle, $\theta_v = 2\ \tan^{-1}[2Z/(X - Y)]$, shown in Figure 4 (e) for the geometry of our nanoSQUID design. The relevant distances, defined in Figure 4(e), are X = 1 μm, the length of the nanoSQUID washer, Y = 27 nm, the distance between the electrodes, and Z = 270 nm, the distance between the two Josephson junctions. For Device B, we determine $\theta_v = 1.01$ rad. For an applied field of 2 T, $B_v = 33$ mT and we estimate the number of vortices penetrating the diamond nanoSQUID electrodes per period to be $N \sim 16$.

In summary, D.C. nano-SQUIDs with Dayem bridge junctions and a physical loop size of 50 nm have been engineered in boron-doped NCD films using precision Ne-ion beam milling. In an un-shunted device, non-hysteretic operation can be maintained in an applied field exceeding 0.1 T with a high flux-to-voltage transfer function, giving a low flux noise $\phi_{noise} = 0.93\ \mu\phi_0/\sqrt{\mathrm{Hz}}$ at 10 kHz, and concurrent spin sensitivity of 7 $\text{spins}/\sqrt{\text{Hz}}$. At increased fields, the period of the modulation in the nanoSQUID output voltage increases considerably, attributed to an additional phase bias induced on the nanoSQUID loop by Abrikosov vortices penetrating the diamond electrodes.

The physical dimensions of the Dayem bridges and nanoSQUID loops fabricated using this approach are significantly different to the effective dimensions of the engineered diamond superconducting device, illustrated by the observation that Dayem bridges with a physical width of about 200 nm operate effectively as Josephson junctions and the effective size of engineered nanoSQUID loops is larger than the physical size. This suggests that ion-beam damage, which gives rise to charged defects at the periphery of milled regions of the NCD film, leads to hole depletion and band structure modification extending laterally by several tens of nanometres into the diamond film. As we have shown, this effect makes it possible to engineer functioning Josephson junctions in diamond using Dayem bridges of physical dimensions larger than the coherence length, but also poses a barrier to significant further miniaturization of diamond SQUIDs unless films with much higher boron concentration are used.

AUTHOR INFORMATION

Corresponding authors

[a] E-mail: M.Bose2@latrobe.edu.au

[b] E-mail: C.Pakes@latrobe.edu.au

Present address

La Trobe University, Bundoora, Victoria 3086, Australia

Notes

The authors declare no competing financial interest.

ACKNOWLEDGEMENTS

This work was performed in part at the Melbourne Centre for Nanofabrication (MCN), and the Materials Characterization and Fabrication Platform (MCFP) at the University of Melbourne, both in the Victorian Node of the Australian National Fabrication Facility (ANFF). D.L.C. is supported by Australian Research Council Discovery Project Grant No. DP190102852.

REFERENCES

[1] C. Granata and A. Vettoliere, Phys. Rep. **614**, 1 (2016).

[2] S.K.H. Lam and D.L. Tilbrook, Appl. Phys. Lett. **82**, 1078 (2003).

[3] Y. Anahory, J. Reiner, L. Embon, D. Halbertal, A. Yakovenko, Y. Myasoedov, M.L. Rappaport, M.E. Huber, and E. Zeldov, Nano Lett. **14**, 6481 (2014).

[4] M. Schmelz, Y. Matsui, R. Stolz, V. Zakosarenko, T. Schönau, S. Anders, S. Linzen, H. Itozaki, and H.G. Meyer, Supercond. Sci. Technol. **28**, (2015).

[5] C.I. Pakes, P.W. Josephs-Franks, R.P. Reed, S.G. Corner, and M.S. Colclough, IEEE Trans. Instrum. Meas. **50**, 310 (2001).

[6] D. Vasyukov, Y. Anahory, L. Embon, D. Halbertal, J. Cuppens, L. Neeman, A. Finkler, Y. Segev, Y. Myasoedov, M.L. Rappaport, M.E. Huber, and E. Zeldov, Nat. Nanotechnol. **8**, 639 (2013).

[7] T. Patel, B. Li, J. Gallop, D. Cox, K. Kirkby, E. Romans, J. Chen, A. Nisbet, and L. Hao, IEEE Trans. Appl. Supercond. **25**, (2015).

[8] C. Granata, A. Vettoliere, B. Ruggiero, M. Russo, M. Fretto, V. Lacquaniti, L. Boarino, and N. De Leo, IEEE Trans. Appl. Supercond. **25**, (2015).

[9] L. Hao and C. Granata, Supercond. Sci. Technol. **30**, (2017).

[10] S.K.H. Lam, J.R. Clem, and W. Yang, Nanotechnology **22**, (2011).

[11] T. Klein, P. Achatz, J. Kacmarcik, C. Marcenat, F. Gustafsson, J. Marcus, E. Bustarret, J. Pernot, F. Omnès, and B.E. Sernelius, Phys. Rev. B **75**, 165313 (2007).

[12] S. Mandal, T. Bautze, O.A. Williams, C. Naud, É. Bustarret, F. Omnès, P. Rodière, T. Meunier, C. Bäuerle, and L. Saminadayar, 1 (2011).

[13] T. Kageura, M. Hideko, I. Tsuyuzaki, A. Morishita, and A. Kawano, 2 (2019).

[14] L. Hao, J.C. MacFarlane, J.C. Gallop, D. Cox, J. Beyer, D. Drung, and T. Schurig, Appl. Phys. Lett. **92**, 2006 (2008).

[15] G.M. Klemencic, D.T.S. Perkins, J.M. Fellows, C.M. Muirhead, R.A. Smith, S. Mandal, S. Manifold, M. Salman, S.R. Giblin, and O.A. Williams, Carbon N. Y. **175**, 43 (2021).

[16] G.C. Tettamanzi, C.I. Pakes, A. Potenza, S. Rubanov, C.H. Marrows, and S. Prawer, Nanotechnology (2009).

[17] D.L. Creedon, Y. Jiang, K. Ganesan, A. Stacey, T. Kageura, H. Kawarada, J.C. McCallum, B.C. Johnson, S. Prawer, and D.N. Jamieson, Phys. Rev. Appl. **10**, 44016 (2018).